Materials Science and Engineering B 164 (2009) 1–5

Contents lists available at ScienceDirect

Materials Science and Engineering B

journal homepage: www.elsevier.com/locate/mseb

Y effects on magnetic and mechanical properties of Fe-based Fe–Nb–Hf–Y–B bulk glassy alloys with high glass-forming ability

Zhilin Long[a,b,*], Yong Shao[c], Fu Xu[a], Hongqing Wei[a], Zhichun Zhang[a], Ping Zhang[a], Xuping Su[b]

[a] Institute of Fundamental Mechanics and Material Engineering, Xiangtan University, Xiangtan, Hunan, 411105, China
[b] Key Laboratory of Materials Design and Preparation Technology of Hunan Province, Xiangtan University, Hunan, 411105, China
[c] Institute for Materials Research, Tohoku University, Sendai 980-8577, Japan

ARTICLE INFO

Article history:
Received 19 August 2008
Received in revised form 24 March 2009
Accepted 1 April 2009

Keywords:
Fe-based bulk metallic glass
Glass-forming ability
Mechanical property
Magnetic property

ABSTRACT

The effects of partial substitution of Y for Fe on the glass-forming ability (GFA), mechanical, thermal and magnetic properties of quinary $Fe_{73-x}Nb_4Hf_3Y_xB_{20}$ (x = 0–3 at.%) alloys were investigated. The replacement of 1–3 at.% Fe by Y increased thermal stability of the supercooled liquid in the Fe–Nb–Hf–Y–B alloys, enabling the fabrication of bulk metallic glasses (BMGs) with diameters up to 4 mm from the original 2 mm. Properties of $Fe_{73-x}Nb_4Hf_3Y_xB_{20}$ BMGs were measured, yielding a rather high saturation magnetization of 1.05–1.22 T, low coercive force of 1.6–3.6 A/m, high compressive fracture strength of 3200–3490 MPa, Yong's modulus (E) of 177–190 GPa and compressive strain before failure ~2%. Furthermore, the role of Y addition on the GFA as well as mechanical and magnetic properties is also discussed.

1. Introduction

Since Fe–metalloid amorphous alloys were found to exhibit good soft-magnetic properties in 1974 [1–3], a large number of studies on the development of soft-magnetic amorphous alloys have been carried out for the subsequent 20 years. However, all the suitable iron-based amorphous metals have a thickness limited to around 30 μm due to their poor glass-forming ability (GFA), so that a cooling rate of almost 10^6 K/s is required for the formation of an amorphous phase [4]. Consequently, the development of Fe-based alloys with high GFA to form thicker amorphous ribbons or bulks has been actively tried in order to extend their industrial applications. Fe-based ferromagnetic bulk metallic glass (BMG) was synthesized for the first time in the Fe–(Al,Ga)–metalloid system in 1995 [5]. Since then, a variety of Fe-based BMGs has been developed, and these BMGs show many advantages including ultrahigh strength, large elastic limit, good formability in the supercooled liquid region, excellent soft-magnetic properties, superior corrosion resistance, low material cost, etc., [6–10]. To date, two classes of Fe-based BMGs have been reported: non-ferromagnetic systems (such as Fe–Mn–Cr–Mo–C–B and Fe–Cr–(Ln,Y)–Mo–C–B) [7,11–14] and soft-magnetic systems (such as Fe–(Al,Ga)–(P,B,C,Si) and Fe–TM (TM = Co,Zr,Nb,Ta,W)–B) [15]. In the cases of non-ferromagnetic systems, the formation of glassy rods with diameters up to 16 mm has been reported in FeCoCrMoCBY system by substituting Fe with a proper amount of Co in a previously reported Fe-based BMG alloy [16]. Although the ferromagnetic alloy systems have been intensively investigated and indeed have huge potential for commercial application, their GFA are not so high compared to non-ferromagnetic BMGs, which is not sufficient yet even for the applications as soft-magnetic materials used for magnetic parts such as valves, clutches, and/or relays. Accordingly, the improvement in the GFA of Fe-based soft-magnetic BMGs has become a key topic in the development of advanced ferromagnetic materials.

Various methods have been proposed and/or used to design BMGs. However, the selection of the constitutional components and the quantification of their contents to obtain good glass formers still remain challenging. Among all readily available methods, microalloying has been proven to be the most effective approach for searching BMGs with a high GFA and high thermal stability against crystallization [17]. In the present study, with the aim of synthesizing a new Fe-based ferromagnetic BMG system with high GFA, and simultaneously exhibiting high fracture strength and good soft-magnetic properties, we examined the effect of substitution of Y for Fe on the improvement on the GFA in the quinary Fe–Nb–Hf–Y–B alloy system, as it has been proven to be effective for the enhancement the GFA of FeB-based BMGs [18,19]. The $Fe_{73}Nb_4Hf_3B_{20}$ alloy was selected as a starting composition, because our recent studies show that this alloy lies in the vicinity of a eutectic point and exhibits the largest supercooled liquid region of 63 K in FeNbHfB system, enabling formation of maximum 2 mm diameter glassy rod. The detailed results on FeNbHfB system will be presented elsewhere.

* Corresponding author. Tel.: +86 732 8293013; fax: +86 732 8292467.
E-mail address: longzl@xtu.edu.cn (Z. Long).

0921-5107/$ – see front matter © 2009 Elsevier B.V. All rights reserved.
doi:10.1016/j.mseb.2009.04.010

2. Experimental

Multi-component Fe-based $Fe_{73-x}Nb_4Hf_3Y_xB_{20}$ (x = 0–3) alloy ingots were prepared by arc melting the mixtures of pure Fe (99.9 mass%), Nb (99.9 mass%), Hf (99.9 mass%) and Y (99.9 mass%) metals, as well as B (99.9 mass%) crystal in an argon atmosphere. The alloy compositions represent nominal atomic percentages. Each ingot was melted at least three times in the arc melter in order to obtain chemical homogeneity. Glassy alloy ribbons with a cross-section of 0.02 mm × 1 mm were produced by melt spinning the pre-alloyed ingots in an argon atmosphere. Bulk glassy alloys in a cylindrical rod form with diameters up to 5 mm and a length of about 50 mm were fabricated by the copper mold casting method. The structure was examined by X-ray diffraction (XRD) with Cu Kα radiation. The thermal stability associated with the glass transition temperature (T_g), onset temperature of crystallization (T_x) and supercooled liquid region ($\Delta T_x = T_x - T_g$) was examined by differential scanning calorimetry (DSC) at a heating rate of 0.67 K/s. The melting (T_m) and liquidus (T_l) temperatures were measured with a differential thermal analyzer (DTA) at a heating rate of 0.67 K/s. The saturation magnetization (I_s) was measured with a vibrating sample magnetometer (VSM) under an applied field of 400 kA/m. The coercive force (H_c) was measured with a B–H loop tracer under a field of 800 A/m. All samples for magnetic properties' measurements were isothermally annealed for 300 s at the temperature of T_g-30 K for improving soft-magnetic properties through structural relaxation. Vickers hardness (H_V) was measured using a pyramidal diamond indenter, applying a load of 0.98 N for 15 s. A minimum of 10 readings was made for each sample; otherwise a sufficient number of tests were performed to achieve a standard deviation of less than 2%. Mechanical properties under a compressive applied load were measured at room temperature with an Instron machine. The gauge dimension of the test sample was 2 mm in diameter and 4 mm in length and the strain rate was 5.0×10^{-4} s^{-1}. At least five samples have been measured to ensure that the results are reproducible.

3. Results

The formation of the amorphous phase was confirmed by XRD experiments in all rapidly solidified $Fe_{73-x}Nb_4Hf_3Y_xB_{20}$ (x = 0–3) alloy ribbons. Fig. 1 shows DSC curves of the melt-spun $Fe_{73-x}Nb_4Hf_3Y_xB_{20}$ (x = 0–3) glassy alloys. It is clearly seen that all alloys exhibit distinguished glass transition, followed by a supercooled liquid region and then two-stage crystallization. The T_g and T_x are marked with arrows in the DSC traces, and T_g, T_x and ΔT_x values are summarized in Table 1. As shown in Fig. 1 and Table 1, one can see that both T_g and T_x increase gradually from 836 to 850 K and 899 to 928 K, respectively, with increasing Y content to 2 at.%. With a further increase of Y content to 3 at.%, T_g remain be unchanged, while T_x slightly decreases to 924 K. On the other hand, ΔT_x shows the same change tendency as T_x. The ΔT_x varied from 63 to 78 K, and shows a maximum value of 78 K at x = 2 at.%. Therefore, it is suggested that the thermal stability of the supercooled liquid increases with increasing Y content to x = 2 at.%, and begins to decrease with a further increase of Y content. The changes in thermal stability of these glassy alloys were further ascertained by comparing their enthalpy of supercooled liquid (ΔH_{endo}), which

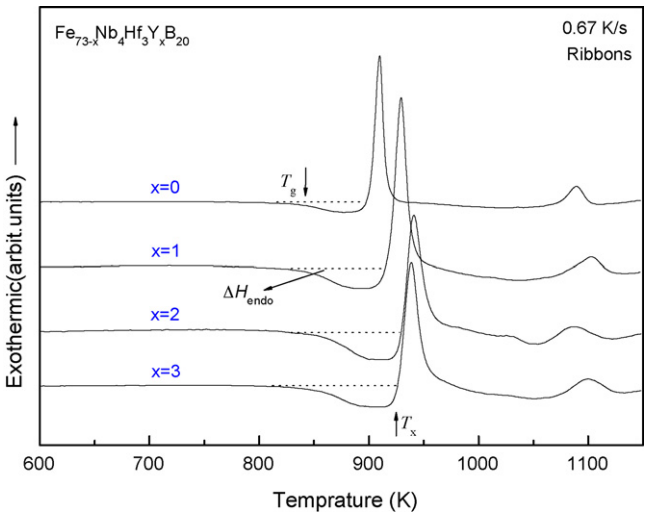

Fig. 1. DSC curves of the melt-spun $Fe_{73-x}Nb_4Hf_xB_{20}$ (x = 0–3) glassy alloy ribbons at a heating rate of 0.67 K/s.

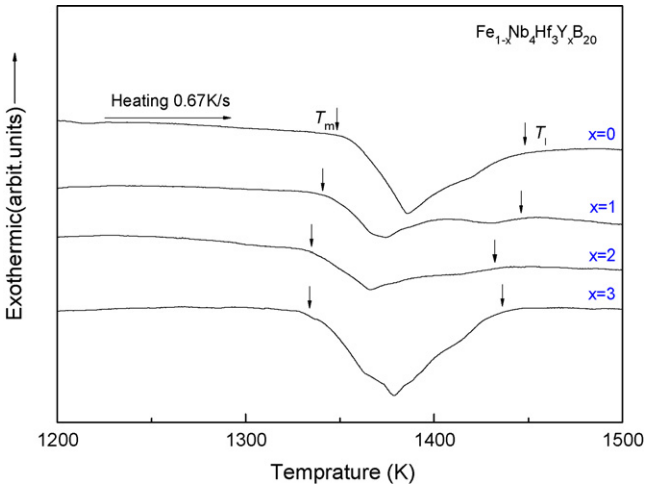

Fig. 2. DTA curves of $Fe_{73-x}Nb_4Hf_3Y_xB_{20}$ (x = 0–3) alloys. The arrows refer to the melting and liquidus temperatures.

were derived from the DSC curves and also marked by the arrow in Fig. 1. It is found that ΔH_{endo} is 15.7 J/g for the Y-free alloy, 18.6 J/g for the 1 at.% Y alloy, 19.7 J/g for the 2 at.% Y alloy and 19.2 J/g for the 3 at.% Y alloy. In view of a higher value of ΔH_{endo}, which is an indictor for the thermal stability of the supercooled liquid, it can be speculated that the alloy with 2 at.% Y in place of Fe has the highest thermal stability of the supercoooled liquid against crystallization compared to other alloys with different Y contents. Fig. 2 shows the melting behaviors of the $Fe_{73-x}Nb_4Hf_3Y_xB_{20}$ (x = 0–3) alloys. The onset melting temperature (T_m) and offset melting temperature (T_l, apparent liquidus temperature) are marked with arrows, and are also summarized in Table 1. It can be seen that Y content affects T_m, T_l and the melting behaviors of these alloys. The free-Y alloy $Fe_{73}Nb_4Hf_3B_{20}$ has a rather high $T_l \sim 1448$ K although it is quite

Table 1
Thermal stability, mechanical and magnetic properties of the as-cast $Fe_{73-x}Nb_4Hf_3Y_xB_{20}$ (x = 0–3) glassy alloys.

Composition (at.%)	T_g (K)	T_x (K)	ΔT_x (K)	T_m (K)	T_l (K)	T_{rg}	γ	ω	D_{max} (mm)	H_v	E' (GPa)	σ_f (MPa)	I_s (T)	H_c (A/m)
$Fe_{73-x}Nb_4Hf_3Y_0B_{20}$	836	899	63	1356	1448	0.5773	0.3936	0.1979	2	1137	177	3200	1.22	3.6
$Fe_{73-x}Nb_4Hf_3Y_1B_{20}$	841	916	75	1341	1446	0.5816	0.4005	0.1827	3	1158	180	3420	1.13	2.4
$Fe_{73-x}Nb_4Hf_3Y_2B_{20}$	850	928	78	1335	1432	0.5936	0.4067	0.1710	4	1163	190	3490	1.08	1.6
$Fe_{73-x}Nb_4Hf_3Y_3B_{20}$	850	924	74	1334	1437	0.5915	0.4040	0.1766	3.5	1160	180	3420	1.05	2.1